中国科学: 物理学 力学 天文学 2025 年 第 55 卷 第 8 期: 286114
SCIENTIA SINICA Physica, Mechanica & Astronomica physcn.scichina.com
《中国科学》杂志社 SCIENCE CHINA PRESS
评 述 非晶态材料物理性能研究专辑

高温非晶合金的研究进展

苏辰, 郭胜锋*

西南大学材料与能源学院, 重庆 400715
*联系人, E-mail: sfguo@swu.edu.cn

收稿日期: 2024-09-24; 接受日期: 2024-12-09; 网络出版日期: 2025-03-14
国家自然科学基金(编号: 52071276, 52471183)和中央高校基本科研业务费专项资金(编号: SWU-XDJH202313)资助项目

摘要 非晶合金因其原子无序排列结构而具有独特的力学、物理和化学性质, 然而, 其在能量上处于热力学亚稳态, 随着服役环境的变化, 会发生结构弛豫甚至晶化, 从而丧失其原有的优异性能, 导致绝大部分非晶合金的使役温度受限. 相对于常规非晶合金, 高温非晶合金(玻璃转变温度通常高于1000 K)具有更高的热稳定性、力学性能、耐腐蚀性及抗氧化性能, 有望在高温、强腐蚀等极端环境下安全服役. 本文系统阐述了近年来高温非晶合金在形成能力、机械性能、化学性质等方面取得的显著进展, 全面评估了已报道高温非晶合金的不同性能, 并对高温非晶合金面临的挑战及未来发展趋势进行了详细讨论, 为推进该类高性能金属材料的工程化应用提供参考和借鉴.

关键词 高温非晶合金, 非晶形成能力, 力学性能, 耐腐蚀性能, 抗氧化性能

PACS: 61.43.Dq, 64.70.Pf, 62.20.-x, 81.40.Np, 81.65.Mq

1 引言

自1960年Duwez等人[1]通过快速凝固技术偶然发现Au-Si二元非晶合金以来, 作为金属材料家族新成员, 非晶合金一经问世便引起了材料和物理学界人员的广泛关注. 与典型的晶态材料不同, 非晶合金的原子排列长程无序, 而具有短程序或中程序结构, 表现出与晶态材料截然不同的物理化学性质. 大部分非晶合金的屈服强度均高于其对应晶态材料[2], 尤其是Co-Ta-B块体非晶合金的强度达到创纪录的6.2 GPa[3]. 另外, 由于非晶合金特殊的原子排列结构, 其不存在容易被腐蚀的位错和晶界等缺陷, 通常展现出优于同成分晶态材料的耐腐蚀性能. 因此, 对非晶合金的深入研究将助力发展新一代优异性能的金属材料, 具有极为重要的意义.

然而, 正是由于非晶合金独特的原子排列结构, 其相比晶态材料具有更高的吉布斯自由能, 在能量上处于热力学亚稳态, 在温度、压力、时间等外界作用下会发生结构弛豫甚至晶化, 从而丧失其原有的优异性能. 因此, 发展具有高稳定性的非晶合金是解决这一问题的关键.

高温非晶合金(High-Temperature Amorphous Al-

引用格式: 苏辰, 郭胜锋. 高温非晶合金的研究进展. 中国科学: 物理学 力学 天文学, 2025, 55: 286114
Su C, Guo S F. Research progress of high-temperature amorphous alloys (in Chinese). Sci Sin-Phys Mech Astron, 2025, 55: 286114, doi: 10.1360/SSPMA-2024-0408

loys)是一类具有较高玻璃转变温度的非晶合金，其玻璃转变温度大多超过1000 K (T_g≥1000 K), 表现出极高的热稳定性. 图1展示了高温非晶合金的一些性能特点[4–7]，由于高温非晶合金具有比常规非晶合金更高的T_g，意味着高温非晶合金内部原子之间的强键合，具有更高的热稳定性、强度、硬度等性能. 其高键合强度，赋予了高温非晶合金在较高温度下，也能保持优异力学和抗氧化性能，例如$Ir_{35}Ni_{25}Ta_{40}$块体非晶合金在1040 K时，依旧保持3.7 GPa的抗压强度，同时在接近T_g的1070 K温度下，并没有发生实质性氧化增重[8], 这是传统金属材料所无法企及的. 本文重点评述近年来发展的高温非晶合金体系, 如Ir, Mo, Os, Ta, W基非晶等，对高温非晶合金的形成规律、力学行为、化学性质等方面进行系统总结和评述，并就高温非晶合金当前面临的挑战和未来发展趋势提出具体的路径, 进一步促进高温非晶合金这类新材料的研发, 拓展其在极端环境下长期服役的安全性.

2　高温非晶合金的形成

非晶形成能力是非晶合金至关重要的参数，人们一直致力于开发强非晶形成能力的大尺寸非晶合金[9–14]，而高温非晶合金对其临界冷却速率要求极高，绝大多数高温非晶合金只能以微米尺寸的粉体或薄膜形式存在. 非晶形成能力相对较差，如Denier van der Gon等人[15]1987年报道的W-Ru，W-Re和Ta-Ir非晶合金，其T_x分别达到775℃，775℃和900℃，但只获得了非晶薄膜；同样，McGlone等人[16]制备的Ta基非晶薄膜，在900℃以上才会发生晶化. 随后，W基、Re基等非晶薄带, 如W-Os-B, W-Ir-B, W-Re-Ru-B, W-Ru-B-Hf也相继问世，其晶化温度均超过1000 K[4]. 2011年，汪卫华课题组[17]报道了Ta基非晶合金，其T_g达到了983 K；2015年，张涛课题组[18]发展了T_g约971 K的Cr基非晶合金；2019年柳延辉课题组[8]开发出T_g超过1000 K的IrNiTaB块体非晶合金，率先提出高温块体非晶合金(High-temperature Bulk Metallic Glasses)这一术语. 随后本课题组[19]报道了首个Mo基块体非晶合金，其T_g约1048 K，高温Mo基非晶合金因其较低的材料成本和良好综合性质受到密切关注. 2023年，李然课题组[20]通过在CoTaB体系中添加Os元素，制备出T_g达1028 K的OsCo基高温非晶合金. 和传统非晶合金相比，高温非晶合金因其高的T_g，合金熔体对其临界冷速要求极高，导致非晶形成尺寸有限. 图2中展示了几种高温非晶合金的玻璃转变温度和临界尺寸[8,9,17–29]，

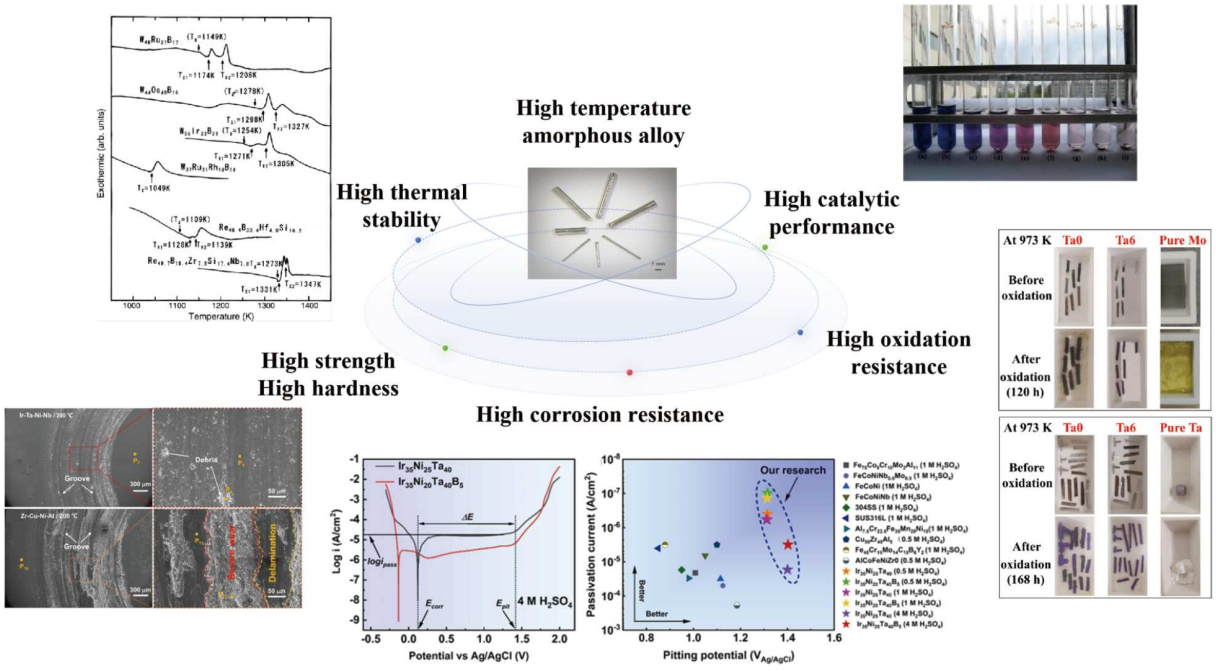

图 1　(网络版彩图)高温非晶合金相关性能[4–7]

Figure 1　(Color online) The related properties of high temperature amorphous alloys [4–7].

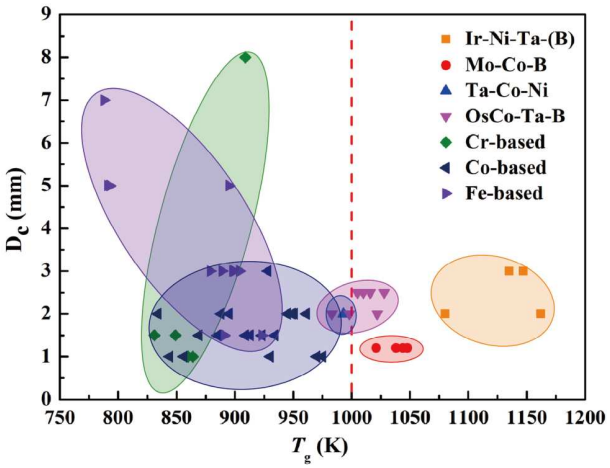

图 2　(网络版彩图)高温非晶合金临界尺寸与玻璃转变温度[8,9,17–29]

Figure 2　(Color online) T_g and critical size of high temperature amorphous alloys [8,9,17–29].

可以发现, 已开发的Ir基、Mo基和OsCo基高温非晶合金棒材最大临界尺寸仅有3 mm, 这极大限制了该类合金的发展. 根据非晶形成理论[30], 合金熔体温度过高, 过冷时间过长, 容易析出晶体相, 导致高温非晶合金形成能力尤为不足. 因此, 解析高温非晶合金的原子局域结构, 澄清高温非晶合金形成的独特机制, 是高温非晶合金未来需要解决的关键任务.

当前对于传统非晶合金的形成机制已经总结出许多半经验方法, 如深共晶点[31]、微合金化[32]、井上三原则[33]、价电子浓度[34]、线团簇模型[35]等. 尽管这些方法在传统非晶合金体系中得到了很好的验证, 但对于高温非晶合金的发展尚待加强.

2.1　高通量磁控溅射成膜筛选

非晶合金对于最优非晶形成能力对应特定化学成分的判定一直是该领域的一大难题. 迄今为止, 具有最大非晶形成能力的非晶合金, 大都是通过反复试错后得到的结果[36–40]. 如何快速确定组元和含量对非晶合金形成能力的影响, 是学者们普遍关注的核心. 近期, 柳延辉课题组[8]通过多靶磁控溅射共沉积技术(图3(a)), 首先制备出含有上千种合金成分的组合样品(图3(b)). 通过高通量结构表征, 如X射线衍射(XRD)和电阻率(图3(c)和(d)), 初步确定非晶形成成分范围; 再结合Ir-Ni-Ta三元相图的等温投影图(图3(e)), 分析认为高

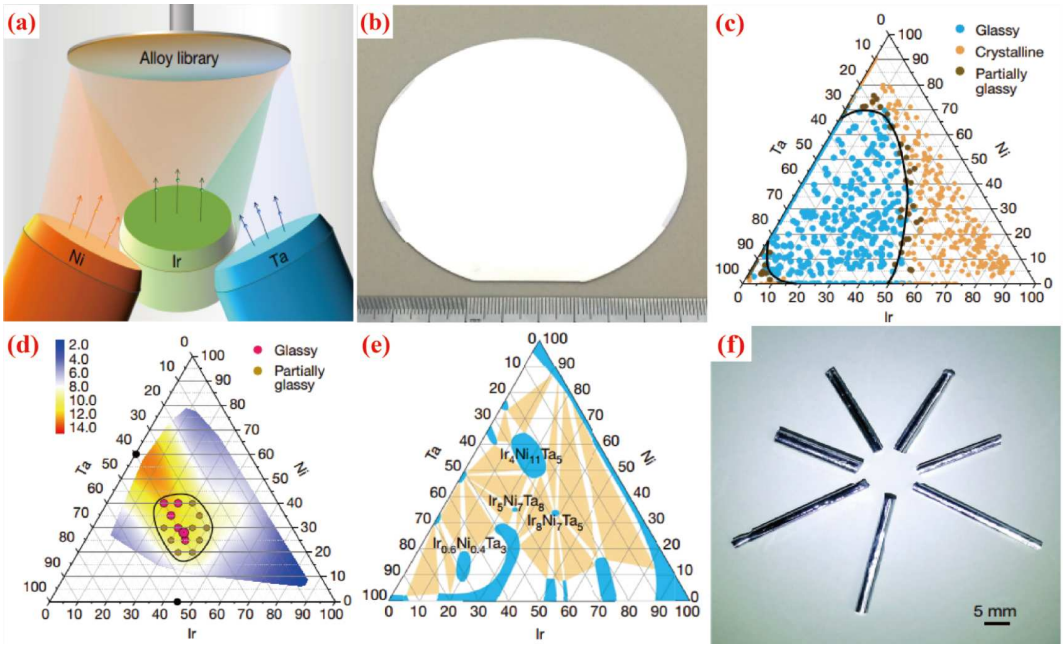

图 3　(网络版彩图)通过多靶磁控溅射共沉积技术制备Ir-Ni-Ta非晶合金[8]. (a) 多靶磁控溅射原理图; (b) 多靶磁控溅射共沉积技术制备的样品; (c) Ir-Ni-Ta三元体系的非晶形成范围; (d) Ir-Ni-Ta平方电阻率变化; (e) Ir-Ni-Ta三元相图的等温投影; (f) Ir-Ni-Ta-(B)棒状样品

Figure 3　(Color online) Ir-Ni-Ta amorphous alloy prepared by magnetron co-sputtering [8]. (a) A schematic diagram of magnetron co-sputtering; (b) the appearance of samples prepared by magnetron co-sputtering; (c) the glass-forming range of the Ir-Ni-Ta ternary alloy; (d) the electrical resistivity of Ir-Ni-Ta; (e) isothermal projection of Ir-Ni-Ta ternary phase diagram; (f) the Ir-Ni-Ta-(B) alloy rods.

温非晶合金的形成能力不仅和熔体共晶点有关，还与界面能和液-固间的成分差异有关，最终通过铜模铸造法获得临界尺寸达3 mm的$Ir_{33}Ni_{28}Ta_{39}$高温非晶合金，如图3(f)所示.

2.2　相近体系相似元素替换

李然课题组[20]以Co-Ta-B体系为基础，根据二元相图，发现Os在Co中表现出较大的固溶度，被认为是部分替代Co的理想元素. 且Os具有极高的熔点和弹性模量，并与Ta，B之间还具有较大的负混合热焓，这有利于增强合金体系的玻璃形成能力，基于此，开发了OsCo基高温非晶合金. 该体系具有高达1028 K的玻璃转变温度(如图4(a))和高达17.6 GPa的维氏硬度. 室温下其抗压强度可达6.0 GPa，在873 K下依然超过4 GPa (如图4(b))

2.3　基于特殊金属间化合物与非晶形成的关联

马恩课题组[41]在对Ni-B，Ni-P和Zr-Pt非晶合金进行结构分析后，发现其存在大量的二十面体团簇或类二十面体团簇结构. 而这种二十面体短-中程有序结构是非晶合金形成过冷液体和准晶体的关键结构单元[35,42,43]. 因此，通过特殊的结构单元进行合理的化学成分设计，可有效地发展良好非晶形成能力合金[44]. 本课题组[19]借助“金属间化合物非晶合金”[45,46]，以特殊金属间化合物σ-Co_2Mo_3相设计Mo基非晶合金，该相具有扭曲的二十面体，可形成高度密堆拓扑结构[47]，其拓扑复杂性对原子协同扩散以及晶体成核和生长造成了巨大障碍，增强了合金过冷液体的稳定性，实现了Mo基块体非晶合金的形成(图5(a)和(b))，通过化学成分调控，确定了高温Mo基非晶形成能力最强的成分区间(图5(c))，其玻璃转变温度均超过1000 K (图5(d)).

3　高温非晶合金力学性质

非晶合金原子无序排列，变形是通过局域原子绝热升温产生剪切带，最终剪切带扩展失稳断裂. 因此，非晶合金的强度接近理论强度. 一般情况下，非晶合金强度可用公式$\sigma = E/50$简单预测[48] (σ为材料的强度，E为材料的杨氏模量)，可以看出高杨氏模量非晶合金往往具有高强度.

对于高温非晶合金，因为本征脆性的影响，其对测试条件极为敏感，很可能尚未达到其本征强度而提前失效[8,49]. 硬度则受外界影响因素较少，且非晶合金的强度和硬度存在很好的线性关系($H_v = 3\sigma_f$)[48]，也可以很好地评估高温非晶合金力学性质. 图6展示了一些典型的非晶合金体系、高温非晶合金以及典型共价晶体材料的杨氏模量和维氏硬度之间的关系. 可以明显看出，无论是非晶合金[3,4,17,19,43,50–53]还是共价晶体[54]，其维氏硬度和杨氏模量都较好地吻合$H_v = 0.06E$这一线性关系. 值得一提的是，高温非晶合金的维氏硬度甚至要高于TiN这类典型的耐磨涂层材料. 高温非晶合金具有较高的硬度，这归结于高温非晶合金内部含有大量的类共价键[35,41]，高温非晶合金含有大量的类金属，可以与金属杂化形成高稳定的共价键. 另一方面，高温

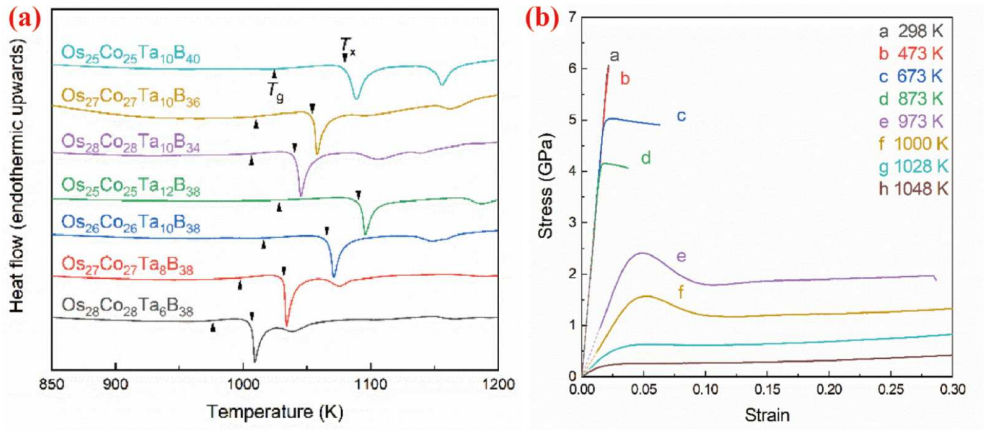

图 4　(网络版彩图) OsCo-Ta-B非晶合金的DSC (a)和力学曲线(b)[20]
Figure 4　(Color online) DSC (a) and strain-stress curves (b) of OsCo-Ta-B amorphous alloy [20].

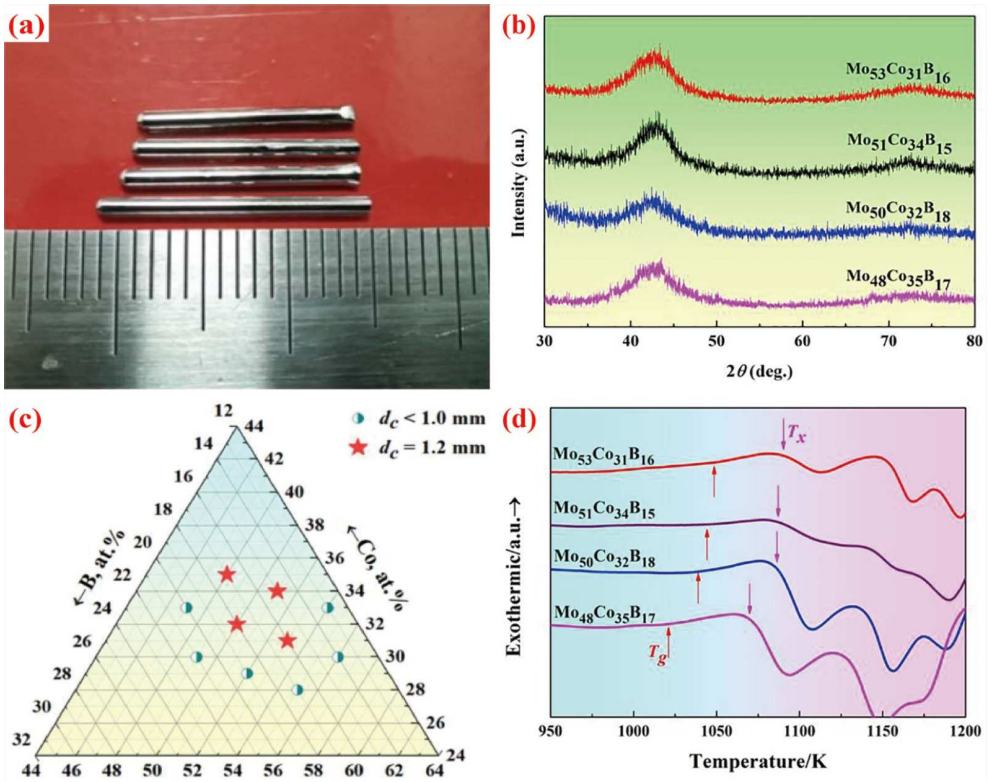

图 5　(网络版彩图) (a) Mo-Co-B非晶合金棒状样品[19]; (b) Mo-Co-B非晶合金XRD图; (c) Mo-Co-B非晶合金形成范围; (d) Mo-Co-B非晶合金DSC图

Figure 5　(Color online) (a) Mo-Co-B amorphous alloy rod [19]; (b) XRD patterns of Mo-Co-B amorphous alloy; (c) the formation range of Mo-Co-B amorphous alloys; (d) DSC of Mo-Co-B amorphous alloy.

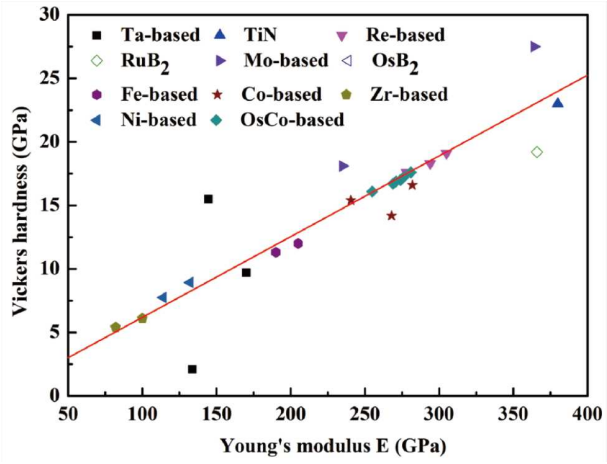

图 6　(网络版彩图)不同非晶合金体系及典型材料的杨氏模量和维氏硬度[3,4,17,19,43,50–54]

Figure 6　(Color online) Young's modulus and Vickers hardness of different amorphous alloys and some typical materials [3,4,17,19,43,50–54].

非晶合金中的难熔金属之间也可形成共价键，大量共价键赋予其超高模量，意味着高温非晶合金在耐磨等领域具有独特优势. 马将课题组[6]发现, Ir-Ta-Ni-Nb高温非晶合金在室温至400℃具有良好的耐磨性，且在750℃下具有比600℃更低的磨损率，而传统的高温合金Inconel 625在同样温度下的磨损率则远高于此[55]，高温非晶合金展现出更为优异的耐磨性能，在航空航天、冶金和核工业具有广阔的应用场景.

含有大量难熔金属不仅仅使得高温非晶合金具有优异的力学性能，同时赋予其高的密度. 图7为一些典型非晶合金体系和高温非晶合金的密度-维氏硬度图[17,18,21,25,29,56–62]，高温非晶合金兼具高硬度和高密度两大优点, 利用高温非晶合金制作穿甲弹弹头, 可以设计具有更大长径比的非晶合金弹芯，增加装药量以提高弹体的初速度. 加上非晶合金自锐性的特点，高温非晶合金弹头可以表现出优异的侵彻穿深性能，作为穿甲弹材料在军工领域极具前景.

高温非晶合金除了优异的室温力学性能外，同样拥有优异的高温力学强度. 对于传统的高温合金，其服役环境温度大多高于600℃，因此往往会发生高温

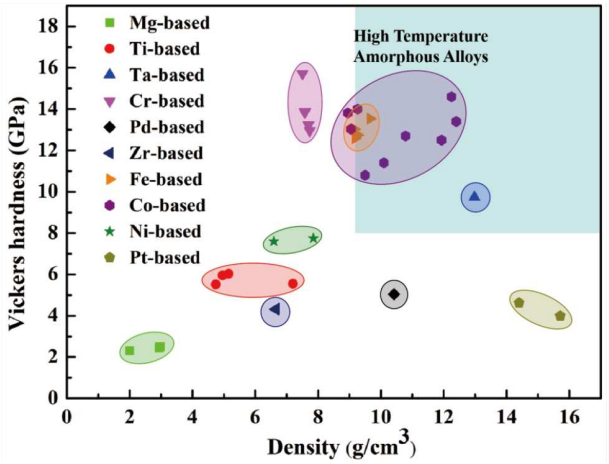

图 7　(网络版彩图)不同非晶合金体系的密度-维氏硬度[17,18,21,25,29,56–62]

Figure 7　(Color online) Density-Vickers hardness of different amorphous alloys [17,18,21,25,29,56–62].

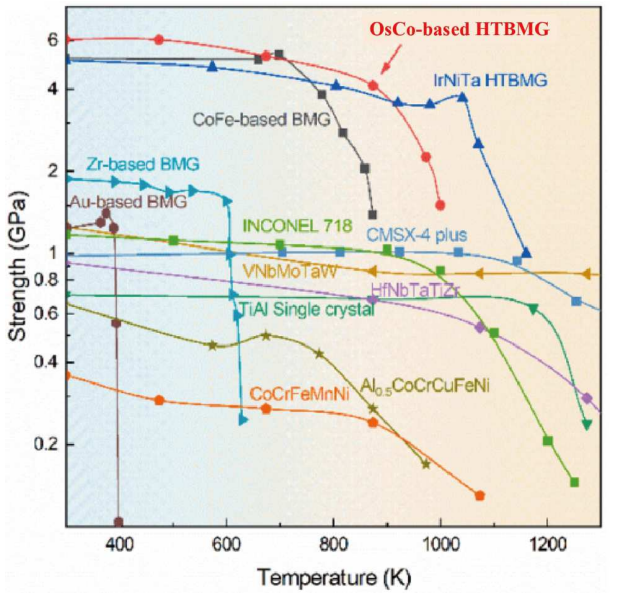

图 8　(网络版彩图)不同高温非晶合金的强度随温度变化[20]

Figure 8　(Color online) Mechanical strength of different high-temperature amorphous alloys at different temperature [20].

软化现象[63]. 图8展示了不同体系高温非晶合金[8,20,64]、高熵合金[65–68]和传统高温合金[69,70]在不同温度下的强度变化[20]. 相较于传统高温合金, 如Inconel 718和TiAl单晶合金. Ir基和OsCo基高温非晶合金不仅在室温具有约5 GPa的超高强度, 即使在800 K左右时, 依然具有4 GPa左右的强度, 远高于传统的高温合金. 尽管非晶合金在温度接近或超过其玻璃转变温度时会发生明显软化, 如Co基非晶合金在700 K以上就会失去其高强度, 但OsCo基和Ir基高温非晶合金在高达1000 K时依旧具有超高强度(超过2 GPa), 而传统的高温合金Inconel 718则在温度超过900 K后, 强度大幅下降, 在1000 K时, 强度只有约800 MPa, 说明研制新型高温非晶合金是发展高温金属结构材料的一种有效途径.

高温非晶合金优异的高温力学强度和其原子键合强度有关. 一般来说, 高温非晶合金的T_g较高, 意味着高温非晶合金更强的原子键合[71]. 当前发展的高温非晶合金均含有大量的类金属, 这些类共价键相互作用明显强于金属键[21,64,72], 能够在较高的环境温度中仍然保持较强的相互作用, 使得高温非晶合金能够在高温下保持较好的抗软化能力.

4　高温非晶合金热力学稳定性

非晶合金作为亚稳态材料, 会自发地通过结构弛豫、晶化等发生向稳态转变而失去非晶态物质优异的性能, 同时在长时间持续加热过程中, 也会发生弛豫老化, 甚至晶化. 当加热到晶化温度时, 原子克服势垒, 发生重排, 短时间内实现形核晶化. 因此, 提高非晶合金晶化温度也是提高其稳定性的有效途径.

与常规非晶合金不同, 高温非晶合金具有极高的晶化温度, 图9总结了一些典型的高温非晶合金玻璃转变温度和晶化温度[8,17–20,23,25,27,73–75]. 从图中可以看出, 以Ir基、Mo基和OsCo基为代表的高温非晶合金普遍具有极高的晶化温度, 甚至超过1000℃, 这也意味着该类合金在高达1000℃的环境下保持非晶结构, 而大多数传统非晶合金在此温度下早已晶化完全甚至熔化. 高温非晶合金极高的晶化温度一方面源于其组成元素具有高熔点, 非晶合金遗传特性赋予其高的晶化温度; 另一方面, 高温非晶合金普遍含有高含量的类金属, 合金原子之间可形成大量的共价键. 共价键的存在使得原子不能通过简单的平移实现晶化, 晶化需克服更高的势垒. 与之相反, 传统的非晶合金对温度极为敏感, 一旦发生晶化, 短时间内就完成晶化过程[76]. 这也反映了高温非晶合金比传统非晶合金更加稳定的结晶动力学和更缓慢的晶化过程. 此外, 缓慢的结晶动力学行为意味着高温非晶合金的结晶过程更容

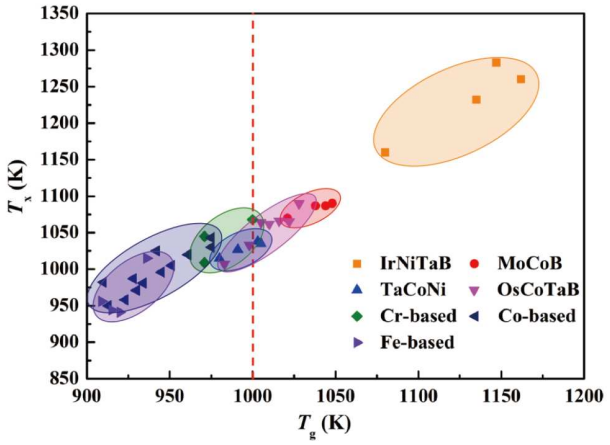

图 9　(网络版彩图)不同非晶合金体系的T_g和T_x[8,17–20,23,25,27,73–75]

Figure 9　(Color online) The T_g and T_x of different amorphous alloys [8,17–20,23,25,27,73–75].

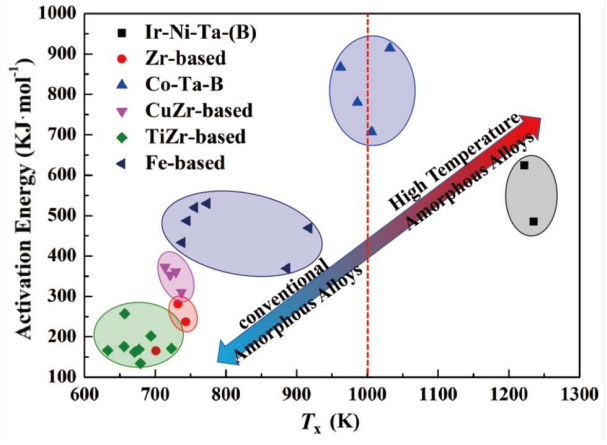

图 10　(网络版彩图)不同非晶合金体系的晶化激活能和晶化温度[8,23,73,74,77–80]

Figure 10　(Color online) The crystallization activation energy and crystallization temperature of different amorphous alloys [8,23,73,74,77–80].

易控制，有望实现制备具有独特功能的纳米晶材料或非晶/纳米晶复合材料.

此外, 过冷液相区的宽度($\Delta T = T_x - T_g$)一定程度上反映了非晶合金的热稳定性. 过冷液相区越宽泛, 表明过冷液相可以在宽泛的温区稳定存在而不致晶化. 当温度超过T_x后, 非晶合金会发生晶化, 但是对于不同体系的非晶合金, 晶化所需要的激活能相差很大. 图10总结了不同非晶合金晶化激活能与初始晶化温度的关联[8,23,73,74,77–80]，可以发现，非晶合金的热稳定性与其熔点有关，低熔点的非晶合金体系，其晶化激活能和晶化温度相应更低，而以Ir基为代表的高温非晶合金却有着较高的晶化温度和较大的晶化激活能，说明高温非晶合金在晶化过程中更难被激活，需要突破更高的能量势垒，这为高温非晶合金在极端环境服役时提供了更多有利的可能.

5　高温非晶合金的耐腐蚀性能

针对非晶合金腐蚀行为的研究, 通常按照金属-金属、金属-类金属分类, 后者往往展现出更高的耐蚀性能. 然而, 仅含类金属的Fe基非晶合金与对应的晶态合金相比，并未展示出更优的耐腐蚀性能[81]. Scully等人[82]指出，具备良好耐蚀性的非晶合金通常具有良好的固溶性, 同时含有大量形成保护性钝化膜的元素.

图11总结了Ir基高温非晶合金[83]以及常见材料在

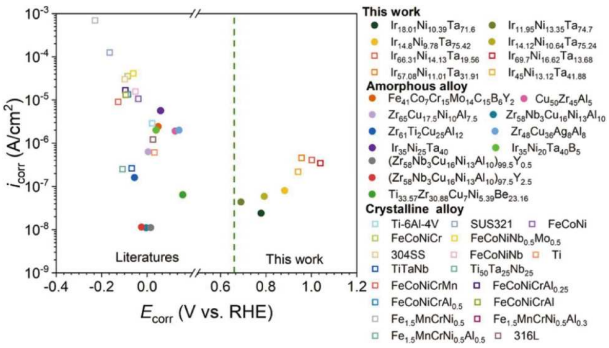

图 11　(网络版彩图)不同非晶合金体系以及常见材料在硫酸溶液中的腐蚀电位和腐蚀电流密度[83]

Figure 11　(Color online) Corrosion potential and corrosion current density of different amorphous alloys and some other alloys in sulfuric acid solution [83].

硫酸溶液中的腐蚀电位和腐蚀电流密度[74–87]. 在这些合金中, Ir-Ni-Ta高温非晶合金具有最高的腐蚀电位和较低的腐蚀电流密度，表明其在硫酸溶液中具有优异的耐蚀性. 这不仅得益于其非晶结构本身，也取决于其化学成分，钽元素形成了致密的钝化层，铱元素以其高稳定性显著提高了合金在硫酸溶液中的自腐蚀电位.

图12总结了304不锈钢、常规耐蚀非晶合金和Ir基高温非晶合金在王水中浸泡不同时间的重量变化[8]. 可以看出, 304不锈钢、Zr基、Fe基非晶合金仅一小时就发生明显腐蚀. 然而, IrNiTa高温非晶合金在112 d后

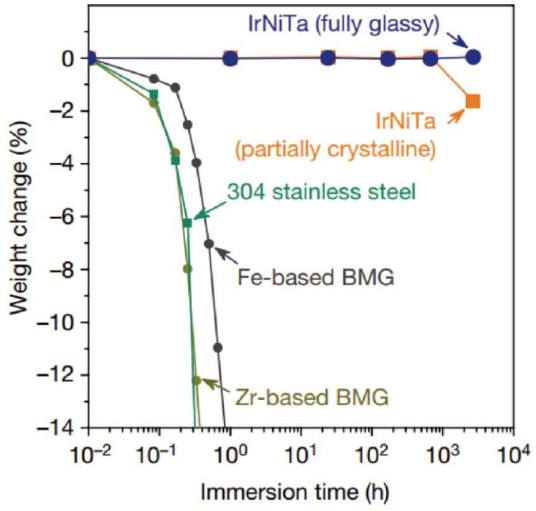

图 12　(网络版彩图)不同非晶合金以及304不锈钢在王水中浸泡不同时间的重量变化[8]

Figure 12　(Color online) Weight changes of different amorphous alloys and 304 stainless steel immersed in aqua regia for different times [8].

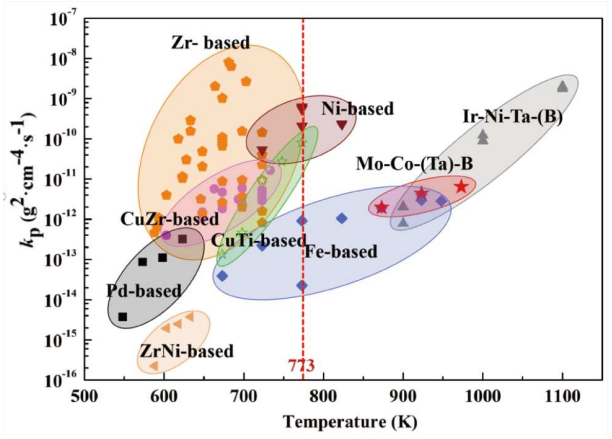

图 13　(网络版彩图)典型非晶合金在不同温度下的氧化速率常数[94]

Figure 13　(Color online) Oxidation rate constants of amorphous alloys at different temperatures [94].

仍未发生明显失重，而部分晶化的IrNiTa高温非晶合金在28 d后才表现出明显的失重，这表明高温非晶合金的确可以承受更为苛刻的腐蚀环境. 随后，王刚和霍军涛课题组[5]研究发现，添加少量B可显著提高Ir-Ni-Ta高温非晶合金在硫酸溶液中的耐蚀性，其自腐蚀电流和钝化电流密度降低了一个数量级. B促进了钝化膜的快速形成，且更加致密，抑制了金属的活性溶解，进一步提高了Ir-Ni-Ta-B高温非晶合金的耐蚀性能.

6　高温非晶合金的高温氧化行为

尽管非晶合金氧化行为是其工程化应用必须面对的问题，但对于非晶合金高温氧化行为(超过773 K)的研究却相对匮乏. 图13总结了各类非晶合金在不同温度的氧化速率常数[88–101]，从图中可知，大部分非晶合金氧化研究温度低于773 K, 仅有Ir基、Mo基以及少量的Fe基和Ni基等高温氧化行为的报道，所有非晶合金均随着温度增加，氧化速率常数增加，抗氧化性随之降低，这和高温下原子的活性和扩散性能增加有关. Pd基[88]、Cu-Zr基[89–91]等非晶合金，高温抗氧化性较差. Ni基非晶在773 K氧化5 h生成了大量带有缺陷的氧化物，导致出现宏观裂纹，同样表现出较差的高温抗氧化性[92].

随着以Ir-Ni-Ta-(B)为代表的高温非晶合金的出现, 拓展了对非晶合金高温氧化行为的研究. 柳延辉课题组[8]发现，Ir-Ni-Ta-(B)非晶合金在连续氧化至接近T_g前均无明显增重现象；王军强课题组[93]研究了B的添加对其在900–1200 K氧化行为的影响，发现由于B的原子半径较小，B原子优先分布在间隙位置，增加了非晶合金晶化的阻碍, 进一步提高了抗氧化性[94,95]. 本课题组[7,94]通过对高温Mo-Co-(Ta)-B非晶合金在873–973 K下进行氧化行为的系统研究, 发现Ta元素能够促使合金形成更细小均匀的氧化表层，同时生成了更致密的富Ta次表层，增加了氧化膜与基体的附着性，降低了次表层的孔洞数量，形成了高致密的尖晶石型氧化物$CoTa_2O_6$，从而有效降低了离子扩散速率，减缓MoCoB非晶合金氧化后期氧化层开裂的倾向，显著提高Mo基非晶合金的高温抗氧化性.

7　高温非晶合金的其他性能

高温非晶合金除具有优异的力学强度和耐腐蚀外，还具有一些特殊性质. 本课题组研究发现[102,103]，Mo基高温非晶合金具有优异的偶氮染料废水催化降解性能. 采用MoCoB高温非晶合金丝材对偶氮染料降解时，发现这类高温非晶合金具有较宽的pH适用范围和较高的反应速率常数，如图14(a). 相比于其他常见的催化材料[104–113]，Mo基高温非晶合金能够在碱性环

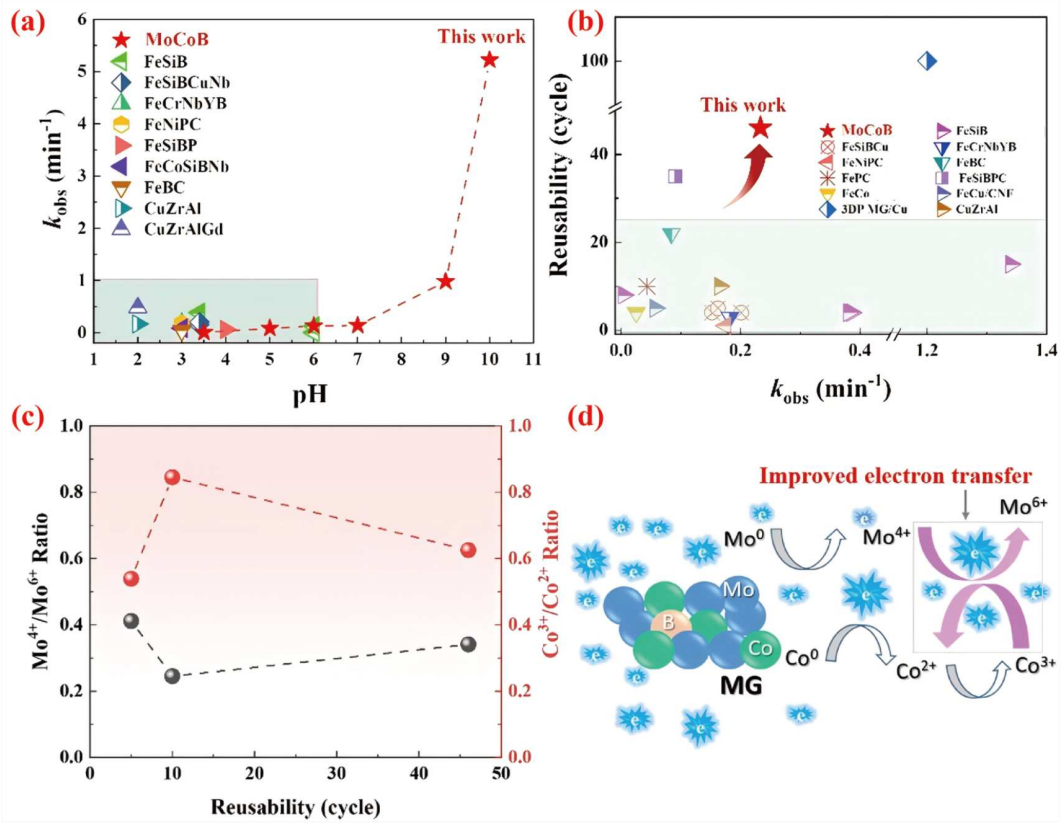

图 14　(网络版彩图) (a) Mo基非晶合金与常见催化材料在不同pH值的催化活性常数; (b) Mo基非晶合金与常见催化材料在降解染料废水时的反应速率常数与循环次数; (c) 不同循环使用次数下Mo/Co元素的价态比例; (d) Mo基非晶合金偶氮染料废水降解机理[103]

Figure 14　(Color online) (a) Catalytic activity constants of Mo-based amorphous alloys at different pH values compared with other common catalytic degradation materials; (b) the reaction rate constant and cycle index of Mo-based amorphous alloy and other catalytic materials; (c) the ratio of Mo/Co elements under different cycles; (d) degradation mechanism of Mo-based amorphous alloy catalyst for wastewater [103].

境中使用, 并且催化活性反应速率常数随着pH值的增加逐渐增加, 且能够兼具良好的催化活性和可重复使用性[104,107,109,110,112,114–116] (图14(b)), 是一种用于染料废水降解的理想催化剂. 分析认为, 其优异的偶氮染料降解能力源于在催化降解过程中, 非晶合金中的Mo元素和Co元素分别为降解反应贡献4个和3个电子. 随后, Mo^{4+}到Mo^{6+}的氧化过程促进Co^{3+}到Co^{2+}的还原过程, 形成双金属内循环机制为降解过程提供大量电子基础, 如图14(c)和(d). 同时, 高温非晶合金在电解水析氢反应方面有着优异的性能, 柳延辉课题组[117]研究Ir-Ni-Ta高温非晶合金薄膜时, 发现其在0.5 mol/L H_2SO_4中对析氢反应表现出高的内在活性和优异的催化稳定性, 优于已报道的非晶合金催化剂, 远高于过渡金属硫化物和磷化物, 可以和其他含贵金属的催化剂相媲美.

除了优异的催化降解性能, Mo基非晶合金还具有良好的超导性能. 1975年, Johnson等人[118]报道了利用熔体快淬得到非晶态合金超导体, 开辟了非晶合金超导研究的新领域. 随后发展了具有超导性的Mo-Ru-B, Mo-Si-B[119–121]非晶合金, 利用Mo基非晶合金更高的晶化温度, 防止温度升高而发生晶化, 获得了更为优异的超导性能.

近期, 为了防止半导体器件中Cu在Si中扩散, 形成高电阻系数的铜硅化物, 宋双喜课题组[122]通过Si和Cu之间制备了一层Mo-Co-B高温非晶合金薄膜. 经过研究发现, 在800℃以下Mo基非晶合金薄膜可以有效阻止Cu与Si之间的扩散, 证明了高温Mo基非晶合金优异的热稳定性和对Cu与Si的扩散阻挡性能, 为Mo基高温非晶合金在集成电路制造业领域的应用提供了良好的借鉴.

8　高温非晶合金的发展与挑战

高温非晶合金作为近来非晶合金家族中的新成员, 具有广泛的应用潜力和深远的学术价值, 要发挥该类材料的突出优势, 拓展其在严苛环境中的长期安全服役, 亟须解决当前面临的几个关键难题.

8.1　揭示高温非晶合金形成机制

目前, 高温非晶合金最大临界尺寸仅为3 mm, 如何发展大尺寸高温非晶合金成为首要解决的问题. 高温非晶合金由于其组元熔点高, 非晶所需临界冷却速率大, 传统的非晶形成理论对高温非晶合金并不完全适用, 这就需要通过对高温非晶合金的形成过程及其结构单元进行深入研究, 不仅可以丰富对非晶合金形成机制的认识, 同时也为开发新的高温非晶合金提供思路.

8.2　快速优化高温非晶合金成分

传统的非晶合金大多通过试错法, 相似元素替代等进行开发新的非晶合金成分, 而高温非晶合金成本高, 非晶形成能力相对较差, 迫切需要开发低成本、高效率的非晶成分优化方法. 材料基因工程、人工智能、机器学习等技术的不断涌现, 极大地推动了材料在研发和应用的速度. 借助先进的材料开发理念, 将极大提升高温非晶合金的研发效率, 降低研发周期与成本.

8.3　高温抗氧化性能

高温非晶合金通常含有大量难熔金属, 而难熔金属本身抗氧化性能较差, 这对高温非晶合金在极端环境长时间服役提出了更为苛刻的要求. 当前对于高温非晶合金的氧化行为研究还处于起始阶段, 仍需进一步深入探究其高温氧化和失效机制, 使其在高温、长时间服役环境下仍能保持稳定的非晶态结构和抗氧化性能.

8.4　高温非晶合金特殊环境中的服役应用

随着科技的不断发展, 需要越来越多能够在太空、核反应堆、熔盐等苛刻环境中长期服役的材料, 如何发挥高温非晶合金这类材料的特殊性质, 拓展其在极端环境中的工程化应用, 还需要进一步深入研究高温非晶合金在极端环境(如强腐蚀、强辐照、高压、强冲击等)下的服役行为以及和环境之间的耦合作用, 拓展高温非晶合金的应用领域.

参考文献

1　Klement W, Willens R, Duwez P. Non-crystalline structure in solidified gold-silicon alloys. Nature, 1960, 187: 869–870
2　Gludovatz B, Hohenwarter A, Catoor D, et al. A fracture-resistant high-entropy alloy for cryogenic applications. Science, 2014, 345: 1153–1158
3　Wang J, Kaban I, Levytskyi V, et al. Ultra-high strength Co-Ta-B bulk metallic glasses: Glass formation, thermal stability and crystallization. J Alloys Compd, 2021, 860: 158398
4　Yoshimoto R, Nogi Y, Tamura R, et al. Fabrication of refractory metal based metallic glasses. Mater Sci Eng-A, 2007, 449-451: 260–263
5　Yang X, Gao M, Liu Y, et al. Superior corrosion resistance of high-temperature Ir-Ni-Ta-(B) amorphous alloy in sulfuric acid solution. Corros Sci, 2022, 200: 110227
6　Sun F, Deng S, Fu J, et al. Superior high-temperature wear resistance of an Ir-Ta-Ni-Nb bulk metallic glass. J Mater Sci Tech, 2023, 158: 121–132
7　Zhou J, Chen F, Zhang C, et al. Effect of Ta on the high temperature oxidation behavior of Mo-based bulk metallic glasses. Surf Coat Tech, 2024, 489: 131108
8　Li M X, Zhao S F, Lu Z, et al. High-temperature bulk metallic glasses developed by combinatorial methods. Nature, 2019, 569: 99–103
9　Li H X, Lu Z C, Wang S L, et al. Fe-based bulk metallic glasses: Glass formation, fabrication, properties and applications. Prog Mater Sci, 2019, 103: 235–318
10　Takeuchi A, Inoue A. Classification of bulk metallic glasses by atomic size difference, heat of mixing and period of constituent elements and its application to characterization of the main alloying element. Mater Trans, 2005, 46: 2817–2829
11　Wang W H, Dong C, Shek C H. Bulk metallic glasses. Mater Sci Eng-R-Rep, 2004, 44: 45–89
12　Lu Z P, Liu C T. A new glass-forming ability criterion for bulk metallic glasses. Acta Mater, 2002, 50: 3501–3512

13 Inoue A. High strength bulk amorphous alloys with low critical cooling rates (*overview*). Mater Trans JIM, 1995, 36: 866–875

14 Inoue A, Takeuchi A. Recent development and application products of bulk glassy alloys. Acta Mater, 2011, 59: 2243–2267

15 Denier van der Gon A W, Barbour J C, de Reus R, et al. Thermal stability of thin-film amorphous W-Ru, W-Re, and Ta-Ir alloys. J Appl Phys, 1987, 61: 1212–1215

16 McGlone J M, Olsen† K R, Stickle W F, et al. TaWSi amorphous metal thin films: Composition tuning to improve thermal stability. MRS Commun, 2017, 7: 715–720

17 Meng D, Yi J, Zhao D Q, et al. Tantalum based bulk metallic glasses. J Non-Cryst Solids, 2011, 357: 1787–1790

18 Xu T, Pang S, Li H, et al. Corrosion resistant Cr-based bulk metallic glasses with high strength and hardness. J Non-Cryst Solids, 2015, 410: 20–25

19 Lai L, Liu T, Cai X, et al. High-temperature Mo-based bulk metallic glasses. Scr Mater, 2021, 203: 114095

20 Bi J, Wei X, Liu X, et al. OsCo-based high-temperature bulk metallic glasses with robust mechanical properties. Scr Mater, 2023, 228: 115336

21 Si J J, Wang T, Wu Y D, et al. Cr-based bulk metallic glasses with ultrahigh hardness. Appl Phys Lett, 2015, 106: 251905

22 Si J J, Chen X H, Cai Y H, et al. Corrosion behavior of Cr-based bulk metallic glasses in hydrochloric acid solutions. Corros Sci, 2016, 107: 123–132

23 Wang J, Li R, Hua N, et al. Co-based ternary bulk metallic glasses with ultrahigh strength and plasticity. J Mater Res, 2011, 26: 2072–2079

24 Ren J, Li Y, Liang X, et al. Role of Fe substitution for Co on thermal stability and glass-forming ability of soft magnetic Co-based Co-Fe-B-P-C metallic glasses. Intermetallics, 2022, 147: 107598

25 Lai L, Ding K, Liu T, et al. Ternary Co-W-B bulk metallic glasses with ultrahigh strength. J Non-Cryst Solids, 2020, 544: 120194

26 Wang J, Wang L, Guan S, et al. Effects of boron content on the glass-forming ability and mechanical properties of Co-B-Ta glassy alloys. J Alloys Compd, 2014, 617: 7–11

27 Dun C, Liu H, Shen B. Enhancement of plasticity in Co-Nb-B ternary bulk metallic glasses with ultrahigh strength. J Non-Cryst Solids, 2012, 358: 3060–3064

28 Liu T, Lai L, Xiao S, et al. Ternary Fe-W-B bulk metallic glasses with ultrahigh thermal stabilities. Mater Sci Eng-A, 2021, 826: 142034

29 Zhang X, Lai L, Xiao S, et al. Effect of W on the thermal stability, mechanical properties and corrosion resistance of Fe-based bulk metallic glass. Intermetallics, 2022, 143: 107485

30 Wang W H, The nature and properties of amorphous matter (in Chinese). Prog Phys, 2013, 33: 177–351 [汪卫华. 非晶态物质的本质和特性. 物理学进展, 2013, 33: 177–351]

31 Turnbull D. Under what conditions can a glass be formed? Contemp Phys, 1969, 10: 473–488

32 Wang W. Roles of minor additions in formation and properties of bulk metallic glasses. Prog Mater Sci, 2007, 52: 540–596

33 Inoue A. Stabilization of metallic supercooled liquid and bulk amorphous alloys. Acta Mater, 2000, 48: 279–306

34 Nagel S R, Tauc J. Nearly-free-electron approach to the theory of metallic glass alloys. Phys Rev Lett, 1975, 35: 380–383

35 Miracle D B. A structural model for metallic glasses. Nat Mater, 2004, 3: 697–702

36 Li Y, Zhao S, Liu Y, et al. How many bulk metallic glasses are there? ACS Comb Sci, 2017, 19: 687–693

37 Tsai P, Flores K M. High-throughput discovery and characterization of multicomponent bulk metallic glass alloys. Acta Mater, 2016, 120: 426–434

38 Ma D, Tan H, Wang D, et al. Strategy for pinpointing the best glass-forming alloys. Appl Phys Lett, 2005, 86: 191906

39 Ding S, Liu Y, Li Y, et al. Combinatorial development of bulk metallic glasses. Nat Mater, 2014, 13: 494–500

40 Li Y, Guo Q, Kalb J A, et al. Matching glass-forming ability with the density of the amorphous phase. Science, 2008, 322: 1816–1819

41 Sheng H W, Luo W K, Alamgir F M, et al. Atomic packing and short-to-medium-range order in metallic glasses. Nature, 2006, 439: 419–425

42 Hirata A, Kang L J, Fujita T, et al. Geometric frustration of icosahedron in metallic glasses. Science, 2013, 341: 376–379

43 Lee G W, Gangopadhyay A K, Hyers R W, et al. Local structure of equilibrium and supercooled Ti-Zr-Ni liquids. Phys Rev B, 2008, 77: 184102

44 Dong C, Wang Q, Chen W, et al. Cluster-based composition rules for ternary alloy systems. J Univ Sci Tech Beijing Miner Metall Mater, 2007, 14: 1–3

45 Schwarz R B, Johnson W L. Formation of an amorphous alloy by solid-state reaction of the pure polycrystalline metals. Phys Rev Lett, 1983, 51: 415–418

46 Wu W F, Li Y. Bulk metallic glass formation near intermetallic composition through liquid quenching. Appl Phys Lett, 2009, 95: 011906

47 Joubert J M. Crystal chemistry and Calphad modeling of the σ phase. Prog Mater Sci, 2008, 53: 528–583

48 Wang W H. The elastic properties, elastic models and elastic perspectives of metallic glasses. Prog Mater Sci, 2012, 57: 487–656

49 Wang Y T, He Q F, Wang Z J, et al. Exceptionally shear-stable and ultra-strong Ir-Ni-Ta high-temperature metallic glasses at micro/nano scales. Sci China Mater, 2022, 65: 501–507

50 Liu F, Yang Q, Pang S, et al. Effect of Mo element on the properties of Fe-Mo-P-C-B bulk metallic glasses. J Non-Cryst Solids, 2009, 355: 1444–1447

51 Lewandowski J J, Gu X J, Shamimi Nouri A, et al. Tough Fe-based bulk metallic glasses. Appl Phys Lett, 2008, 92: 091918

52 Afonso C R M, Bolfarini C, Botta W J, et al. Formation and microstructure of $Ni_{62-x}Nb_{38}Ti_x$ (x = 3, 6, 10 at.%) bulk metallic glasses. Int J Mater Res, 2012, 103: 1096–1101

53 Huang Z, Tao P, Long Z, et al. Effect of Ti addition on mechanical properties of Zr-based bulk metallic glasses. J Non-Cryst Solids, 2023, 601: 122075

54 Chung H Y, Weinberger M B, Yang J M, et al. Correlation between hardness and elastic moduli of the ultraincompressible transition metal diborides RuB_2, OsB_2, and ReB_2. Appl Phys Lett, 2008, 92: 261904

55 Wang Y, Jia Z, Ji J, et al. Tribo-oxidation mechanism of gradient nanostructured Inconel 625 alloy during high-temperature wear. Wear, 2024, 558-559: 205581

56 Li H, Pang S, Liu Y, et al. Biodegradable Mg-Zn-Ca-Sr bulk metallic glasses with enhanced corrosion performance for biomedical applications. Mater Des, 2015, 67: 9–19

57 Liens A, Etiemble A, Rivory P, et al. On the potential of bulk metallic glasses for dental implantology: Case study on $Ti_{40}Zr_{10}Cu_{36}Pd_{14}$. Materials, 2018, 11: 249

58 Gong P, Deng L, Jin J, et al. Review on the research and development of Ti-based bulk metallic glasses. Metals, 2016, 6: 264

59 Gong P, Li F, Jin J. Preparation, characterization, and properties of novel Ti-Zr-Be-Co bulk metallic glasses. Materials, 2020, 13: 223

60 Liu Y, Hata S, Wada K, et al. Thermal, mechanical and electrical properties of Pd-based thin-film metallic glass. Jpn J Appl Phys, 2001, 40: 5382–5388

61 Mao J, Zhang H F, Fu H M, et al. Effects of casting temperature on mechanical properties of Zr-based metallic glasses. Mater Sci Eng-A, 2010, 527: 981–985

62 Lai L, He R, Ding K, et al. Ternary Co-Mo-B bulk metallic glasses with ultrahigh strength and good ductility. J Non-Cryst Solids, 2019, 524: 119657

63 Gudivada G, Pandey A K. Recent developments in nickel-based superalloys for gas turbine applications: Review. J Alloys Compd, 2023, 963: 171128

64 Inoue A, Shen B, Koshiba H, et al. Cobalt-based bulk glassy alloy with ultrahigh strength and soft magnetic properties. Nat Mater, 2003, 2: 661–663

65 Senkov O N, Wilks G B, Scott J M, et al. Mechanical properties of $Nb_{25}Mo_{25}Ta_{25}W_{25}$ and $V_{20}Nb_{20}Mo_{20}Ta_{20}W_{20}$ refractory high entropy alloys. Intermetallics, 2011, 19: 698–706

66 Senkov O N, Scott J M, Senkova S V, et al. Microstructure and elevated temperature properties of a refractory TaNbHfZrTi alloy. J Mater Sci, 2012, 47: 4062–4074

67 Tsai C W, Tsai M H, Yeh J W, et al. Effect of temperature on mechanical properties of $Al_{0.5}$CoCrCuFeNi wrought alloy. J Alloys Compd, 2010, 490: 160–165

68 Otto F, Dlouhý A, Somsen C, et al. The influences of temperature and microstructure on the tensile properties of a CoCrFeMnNi high-entropy alloy. Acta Mater, 2013, 61: 5743–5755

69 Chen G, Peng Y, Zheng G, et al. Polysynthetic twinned TiAl single crystals for high-temperature applications. Nat Mater, 2016, 15: 876–881

70 Miracle D B, Senkov O N. A critical review of high entropy alloys and related concepts. Acta Mater, 2017, 122: 448–511

71 Wang W H. Correlations between elastic moduli and properties in bulk metallic glasses. J Appl Phys, 2006, 99: 093506

72 Guo S F, Qiu J L, Yu P, et al. Fe-based bulk metallic glasses: Brittle or ductile? Appl Phys Lett, 2014, 105: 161901

73 Su C, Chen Y, Yu P, et al. Linking the thermal characteristics and mechanical properties of Fe-based bulk metallic glasses. J Alloys Compd, 2016, 663: 867–871

74 Zhang J, Su C, Zhang X, et al. Fe-based bulk metallic glass with high thermal stability and corrosion resistance. J Non-Cryst Solids, 2024, 643:

123176
75 Xu T, Pang S, Zhang T. Glass formation, corrosion behavior, and mechanical properties of novel Cr-rich Cr-Fe-Mo-C-B-Y bulk metallic glasses. J Alloys Compd, 2015, 625: 318–322
76 Schroers J, Wu Y, Busch R, et al. Transition from nucleation controlled to growth controlled crystallization in $Pd_{43}Ni_{10}Cu_{27}P_{20}$ melts. Acta Mater, 2001, 49: 2773–2781
77 Li Y C, Zhang C, Xing W, et al. Design of Fe-based bulk metallic glasses with improved wear resistance. ACS Appl Mater Interfaces, 2018, 10: 43144–43155
78 Gong P, Wang X, Yao K. Effects of alloying elements on crystallization kinetics of Ti-Zr-Be bulk metallic glass. J Mater Sci, 2016, 51: 5321–5329
79 Hao Z, Qin K, Song K, et al. Effect of Fe addition on glass-forming ability, thermal stability of B2 CuZr phase and crystallization kinetics for CuZr-based amorphous alloys. J Mater Res Tech, 2021, 15: 6464–6475
80 Liu Z Y, Wu Y, Li H X, et al. Alloying effects of iridium on glass formation and glass-forming ability of the Zr-Cu-Al system. J Mater Res, 2009, 24: 1619–1623
81 Naka M, Hashimoto K, Masumoto T. Change in corrosion behavior of amorphous Fe-P-C alloys by alloying with various metallic elements. J Non-Cryst Solids, 1979, 31: 355–365
82 Scully J R, Gebert A, Payer J H. Corrosion and related mechanical properties of bulk metallic glasses. J Mater Res, 2007, 22: 302–313
83 Hu L, Li F, Xie W, et al. Combinatorial investigation on corrosion resistance of Ir-Ni-Ta alloys. Corros Sci, 2024, 234: 112153
84 Tam M K, Shek C H. Crystallization and corrosion resistance of $Cu_{50}Zr_{45}Al_5$ bulk amorphous alloy. Mater Chem Phys, 2006, 100: 34–37
85 Chen W Y, Chen Y H, Li W P, et al. Passivation evolution of Ti-Ta-Nb medium-entropy sputtered thin films in sulfuric acid solution. Appl Surf Sci, 2022, 576: 151824
86 Yang Y J, Jin Z S, Ma X Z, et al. Comparison of corrosion behaviors between Ti-based bulk metallic glasses and its composites. J Alloys Compd, 2018, 750: 757–764
87 Lee C P, Chang C C, Chen Y Y, et al. Effect of the aluminium content of $Al_xCrFe_{1.5}MnNi_{0.5}$ high-entropy alloys on the corrosion behaviour in aqueous environments. Corros Sci, 2008, 50: 2053–2060
88 Kai W, Ren I F, Barnard B, et al. Oxidation behavior of a $Pd_{43}Cu_{27}Ni_{10}P_{20}$ bulk metallic glass and foam in dry air. Metall Mater Trans A, 2010, 41: 1720–1725
89 Kai W, Ho T H, Hsieh H H, et al. Oxidation behavior of CuZr-based glassy alloys at 400°C to 500°C in dry air. Metall Mater Trans A, 2008, 39: 1838–1846
90 Cao W H, Zhang J L, Shek C H. The oxidation behavior of $Cu_{42}Zr_{42}Al_8Ag_8$ bulk metallic glasses. J Mater Sci, 2012, 48: 1141–1146
91 Kai W, Ren I F, Kao P C, et al. Air - oxidation of a $Cu_{45}Zr_{45}Al_5Ag_5$ bulk metallic glass. Adv Eng Mater, 2009, 11: 380–386
92 Yamasaki M, Habazaki H, Asami K, et al. Oxidation behavior of amorphous Ni-Zr and Ni-Zr-Sm alloys. J Electrochem Soc, 2000, 147: 4502–4506
93 Han F, Chen Y, Liu Y H, et al. High temperature oxidation behaviors of Ir-Ni-Ta-(B) metallic glass. Corros Sci, 2022, 205: 110420
94 Zhou J, Chen F, Lai L, et al. High temperature oxidation behavior of MoCoB metallic glass. Mater Charact, 2024, 211: 113858
95 Dhawan A, Mathur S, Vyas R, et al. Air oxidation of the bulk amorphous alloy $Zr_{46.75}Ti_{8.25}Cu_{7.5}Ni_{10}Be_{27.5}$ studied by using a TGA. Phys Scr, 2010, 82: 045602
96 Lu S, Sun S, Tu G, et al. The effect of yttrium addition on the air oxidation behavior of Zr-Cu-Ni-Al bulk metallic glasses at 400–500 °C. Corros Sci, 2018, 137: 53–61
97 Kai W, Lin P C, Chen W S, et al. Air-oxidation of a $Zr_{50}Cu_{43}A_{17}$ bulk metallic glass at 400–500°C. Corros Sci, 2012, 64: 98–104
98 Liu L, Chan K C. Oxidation of $Zr_{55}Cu_{30}Al_{10}Ni_5$ bulk metallic glass in the glassy state and the supercooled liquid state. Appl Phys A, 2004, 80: 1737–1744
99 Kai W, Hsieh H H, Nieh T G, et al. Oxidation behavior of a Zr-Cu-Al-Ni amorphous alloy in air at 300–425°C. Intermetallics, 2002, 10: 1265–1270
100 Dhawan A, Raetzke K, Faupel F, et al. Study of oxidation behaviour of Zr-based bulk amorphous alloy $Zr_{65}Cu_{17.5}Ni_{10}Al_{7.5}$ by thermogravimetric analyser. Bull Mater Sci, 2001, 24: 281–283
101 Hsieh H H, Kai W, Huang R T, et al. Effect of Zr-content on the oxidation and phase transformation of Zr-base amorphous alloys in air.

Intermetallics, 2004, 12: 1089–1096
102 Tang M, Lai L, Ding D, et al. Rapid degradation of direct blue dye by Co-based amorphous alloy wire. J Non-Cryst Solids, 2022, 576: 121282
103 Tang M, Lai L, Su C, et al. MoCoB metallic glass microwire catalysts for highly efficient and pH-universal degradation of wastewater. npj Mater Degrad, 2023, 7: 73
104 Miao F, Wang Q, Zeng Q, et al. Excellent reusability of FeBC amorphous ribbons induced by progressive formation of through-pore structure during acid orange 7 degradation. J Mater Sci Tech, 2020, 38: 107–118
105 Li Z, Qin X, Zhu Z, et al. Cu-based metallic glass with robust activity and sustainability for wastewater treatment. J Mater Chem A, 2020, 8: 10855–10864
106 Zhang C Q, Zhu Z W, Zhang H F, et al. Rapid reductive degradation of azo dyes by a unique structure of amorphous alloys. Chin Sci Bull, 2011, 56: 3988–3992
107 Jia Z, Kang J, Zhang W C, et al. Surface aging behaviour of Fe-based amorphous alloys as catalysts during heterogeneous photo Fenton-like process for water treatment. Appl Catal B-Environ, 2017, 204: 537–547
108 Liu P, Zhang J L, Zha M Q, et al. Synthesis of an Fe rich amorphous structure with a catalytic effect to rapidly decolorize azo dye at room temperature. ACS Appl Mater Interfaces, 2014, 6: 5500–5505
109 Yang W, Wang Q, Li W, et al. A novel thermal-tuning Fe-based amorphous alloy for automatically recycled methylene blue degradation. Mater Des, 2019, 161: 136–146
110 Liang S X, Zhang W, Wang W, et al. Surface reactivation of FeNiPC metallic glass: A strategy for highly enhanced catalytic behavior. J Phys Chem Solids, 2019, 132: 89–98
111 Deng Z, Zhang X H, Chan K C, et al. Fe-based metallic glass catalyst with nanoporous surface for azo dye degradation. Chemosphere, 2017, 174: 76–81
112 Zhao B, Zhu Z, Qin X D, et al. Highly efficient and stable CuZr-based metallic glassy catalysts for azo dye degradation. J Mater Sci Tech, 2020, 46: 88–97
113 Jiang J L, Jia Z, He Q, et al. Synergistic function of iron and cobalt in metallic glasses for highly improving persulfate activation in water treatment. J Alloys Compd, 2020, 822: 153574
114 Ge Y X, Zhu P Y, Yu Y, et al. Remarkably enhanced Fenton-like catalytic activity and recyclability of Fe-based metallic glass by alternating magnetic field: Mechanisms and industrial applications. J Mater Chem A, 2022, 10: 23314–23322
115 Ganiyu S O, Huong Le T X, Bechelany M, et al. A hierarchical CoFe-layered double hydroxide modified carbon-felt cathode for heterogeneous electro-Fenton process. J Mater Chem A, 2017, 5: 3655–3666
116 Wang J, Liu C, Li J, et al. *In-situ* incorporation of iron-copper bimetallic particles in electrospun carbon nanofibers as an efficient Fenton catalyst. Appl Catal B-Environ, 2017, 207: 316–325
117 Wang Z J, Li M X, Yu J H, et al. Low‐iridium‐content IrNiTa metallic glass films as intrinsically active catalysts for hydrogen evolution reaction. Adv Mater, 2020, 32: 1906384
118 Johnson W L, Poon S J, Duwez P. Amorphous superconducting lanthanum-gold alloys obtained by liquid quenching. Phys Rev B, 1975, 11: 150–154
119 Johnson W L, Williams A R. Structure and properties of transition-metal-metalloid glasses based on refractory metals. Phys Rev B, 1979, 20: 1640–1655
120 Clemens B M, Johnson W L. Surface flux pinning in superconducting amorphous $(Mo_{0.6}Ru_{0.4})B_{18}$. J Appl Phys, 1982, 53: 7612–7614
121 Inoue A, Sakai S, Kimura H, et al. Superconductivity of MoSiB and WSiB amorphous alloys obtained by liquid quenching. Scripta Metall, 1980, 14: 235–239
122 Wang C, Zhang Z, Wang C, et al. Thermally stable Mo-Co-B thin film metallic glass as a potential diffusion barrier in Cu/Si contact system. Intermetallics, 2024, 169: 108296

Research progress of high-temperature amorphous alloys

SU Chen & GUO ShengFeng*

School of Materials and Energy, Southwest University, Chongqing 400715, China
**Corresponding author (email: sfguo@swu.edu.cn)*

Amorphous alloys have unique mechanical, physical and chemical properties due to their disordered atomic arrangement. However, a thermodynamic metastable state, the amorphous alloys would occur structural relaxation and even crystallization with the environment changes, lead to the most parts of the amorphous alloy are limited application far below the high service temperature. Compared with the conventional amorphous alloys, high-temperature amorphous alloys (the glass transition temperature is usually higher than 1000 K) which have much higher thermal stability, mechanical properties, corrosion resistance and antioxidant properties, are expected to be applied in the extreme environments, such as high temperature and strong corrosion environment. This review paper expounds the remarkable progress of high-temperature amorphous alloys in the glass formation ability, mechanical properties, chemical properties and other performance. The different performance of high-temperature amorphous alloys previously reported are comprehensively appraised and discussed. The challenges and future development trends of high-temperature amorphous alloys are also discussed to provide the reference for the application of this high performance metals.

high-temperature amorphous alloy, glass forming ability, mechanical property, corrosion resistance, oxidation resistance

PACS: 61.43.Dq, 64.70.Pf, 62.20.-x, 81.40.Np, 81.65.Mq

doi: 10.1360/SSPMA-2024-0408